JOURNAL OF SPACECRAFT AND ROCKETS
Vol. 32, No. 1, January–February 1995

Analysis of a Terminal Landing on Mars

Dan G. Tuckness*
University of Texas at Arlington, Arlington, Texas 76019-0018

This study consists of a preliminary performance and sensitivity assessment of trajectory and guidance capabilities of a Mars terminal landing phase. The phase begins with the end of the entry phase, which is at parachute deployment. Therefore, the trajectory investigated in this study starts at parachute deployment and continues through parachute jettison and finally propulsive deceleration and maneuvering to a specified landing site. Various landing navigation maneuver schemes and environmental conditions for the lander are investigated and their performance analyzed. Effects of atmospheric density and surface wind deviations on landing guidance are investigated using stochastic wind and density models. Simulation shows that the lander guidance is robust to wind and density dispersions. Density dispersions are found to be more critical for a precision landing than wind dispersions. Also, because of the aerodynamic characteristics of current aeroshell vehicle designs, very little terminal maneuvering is allowed for navigation.

Nomenclature

A_i = current acceleration, m/s^2
A_{it} = terminal acceleration requirement, m/s^2
A_0 = first coefficient of the acceleration polynomial (equal to the acceleration at t_0), m/s^2
D_i = partial derivative of the jerk with respect to T_{go}
F_i = jerk (time derivative of acceleration)
J_{it} = terminal jerk requirement, m/s^3
J_0 = second coefficient of the acceleration polynomial (equal to the jerk at t_0), m/s^3
L_u = horizontal wind-gust scale length, m
L_v = side wind-gust scale length, m
L_w = vertical wind-gust scale length, m
R_i = current position, m
R_{it} = terminal position requirement, m
R_0 = position, m
S_0 = third coefficient of the acceleration polynomial [equal to the snap (second time derivative of acceleration) at t_0], m/s^4
T_{go} = time to go, s
T_x, T_y, T_z = thrust commands in the vehicle local (x, y, z) coordinate system, m/s^2
T/W = lander thrust-to-weight ratio
t = current time, s
t_0 = initial time, s
U_0 = horizontal vehicle speed, m/s^2
V_i = current velocity, m/s^2
V_{it} = terminal velocity requirement, m/s^2
V_0 = velocity, m/s^2
β = frequency of density perturbation, cycles/m
Δh = altitude stepsize, m
σ_u = horizontal wind-gust standard deviation, m/s^2
σ_v = side wind-gust standard deviation, m/s^2
σ_w = vertical wind gust standard deviation, m/s^2
σ_ρ = standard deviation of the density perturbation, kg/m^3
$\Phi_n(\omega)$ = power spectral density function of wind-gust model, m/s
$\phi_{\rho\rho}$ = autocorrelation of random-density model, kg^2/m^6
ω = observed angular frequency, s^{-1}

Received Sept. 7, 1993; revision received March 30, 1994; accepted for publication Sept. 12, 1994.

*Assistant Professor, Department of Mechanical and Aerospace Engineering, Box 19018. Member AIAA.

Introduction

FUTURE Mars landers must be tolerant of environmental trajectory dispersions such as changing winds, abnormal atmospheric density changes, and navigation errors. All of these disturbances contribute to landing dispersions. The lander's mission must be designed to accommodate the disturbances or have the ability to sense them so that it can alter its trajectory in order to avoid hazards. In turn, this would allow the lander to navigate safely to the desired landing site while meeting landing requirements.

In order to study the capabilities of a Mars lander, a baseline mission (vehicle and proposed vehicle trajectory) must be selected. The Mars Rover Sample Return (MRSR) mission, which was canceled in 1990, is an excellent representation of future Mars missions. It is used as the baseline mission for this study with the understanding that it is representative of future missions such as the manned Mars missions.

Future missions such as the MRSR mission differ in several areas from previous missions. A major difference between the landing capabilities of the MRSR mission lander and previous Martian mission landers, such as Viking lander, is in obstacle (or hazard) avoidance and precision landings. This paper investigates hazard avoidance and precision landing techniques and compares them with navigation techniques used on previous missions. The Viking missions were only designed to perform a soft landing and had no onboard hazard avoidance capabilities (no active downrange and crossrange guidance capabilities). Therefore, it risked the possibility of mission failure if the lander had touched down onto an obstacle greater than the tolerance capabilities of the lander design. In order to reduce the possibility of mission landing failure, the Viking landers were directed to landing areas with a low probability of hazards.

Today there are more stringent landing requirements. For example, rocks with diameters less than 1 m and surface slopes less than 15 deg over 10 m were considered to be baseline requirements for proposed missions such as the MRSR mission.[1–4] New lander designs may have the capability to avoid obstacles that could cause a landing failure by intelligently scanning for obstacles using navigation sensors such as synthetic aperture radar (SAR). This will give future mission planners the ability to design missions where the landers can land in rougher terrain that may have a greater geological interest.

Three types of error contribute to landing error. These are dispersions to a nominal ideal guidance flight-path control, initial knowledge of the navigated state, and sensor accumulated error. There are two calculated components that reflect these deviations. First is the difference between the actual and the nominal trajectory. Second is the difference between the current and the actual trajectory. The latter does not apply to the ideal guidance errors. That is, navigation errors are assumed to be zero (perfect navigation).

A large contributor to the guidance control error is from environmental dispersions. This paper investigates these dispersions, with concentration on assessing the capability of the lander in removing guidance control error subject to mission constraints. Guidance and control capability of an MRSR vehicle is discussed and analyzed. A study is also conducted to assess the maneuverability of the vehicle during the terminal stages of its flight. Some navigation methods, such as Synthetic Aperture Radar (SAR), require the vehicle to perform certain maneuvers near its final destination in order to navigate properly. Therefore, navigation capabilities (or the capability of the lander in removing navigation errors) are indirectly a function of the maneuverability of the lander.

Baseline Lander-System Design and Initial Conditions

Lander-System Vehicle Design

The baseline configurations for this study were taken from the NASA MRSR Pre-Phase A study[5] and consist of the following lander-system design. A brief description of the lander system used in this study is as follows.

1) Aeroshell: The representative entry aeroshell vehicle is the JSC configuration M with a symmetrical biconic shape. It provides a lift/drag ratio of 0.98 at a trim angle of attack of 27 deg. The mass and ballistic coefficient of the vehicle are 4082 kg and 397 kg/m^2, respectively.

2) Parachute system: The baseline parachute type is a disk-gap-band (DGB) parachute. This is the type of parachute developed by the Planetary Entry Parachute Program[6] (PEPP) that determined the Viking parachute design. A DGB parachute was baselined because of its proven applicability to a Mars landing problem, the abundance of engineering data about it, and its high-Mach-number stability combined with good drag performance. Mass estimates used in the analysis were based on the parachute data presented in Refs. 3 and 5.

3) Lander vehicle: The terminal descent engine(s) must have thrust magnitude and thrust direction control in order to maneuver around obstacles.

Lander-System Guidance Design

Azimuth Guidance

The azimuth guidance phase begins at the end of the entry guidance phase at about 25 km in altitude and 20 km downrange from the touchdown point. It involves a simple guidance scheme where the aeroshell bank command is a direct function of the azimuth measurement angle to the touchdown point (or area). The bank command is multiplied by a gain that is a function of the distance to the target. Its sole purpose is to align the vehicle velocity vector of the aeroshell towards the touchdown point. Because the bank command is a direct function of the azimuth to the touchdown point, it produces a much more accurate (or more sensitive) command than the entry guidance.

Parachute Guidance

The only trajectory control available during the parachute phase is the timing of parachute deployment and jettison.

Landing Guidance

The power guidance implemented for this study is based on the explicit guidance equations used for the Lunar Excursion Module (LEM).[7–10] The LEM algorithm models the acceleration of the vehicle as a second-order polynomial function of the time remaining to the target. The coefficients of the relative acceleration polynomials are computed by constraining the trajectory to the initial and final boundary conditions (state vectors). For a landing problem, the final boundary condition (target contact) comprises the vehicle relative acceleration, velocity, and position at touchdown:

$$A = A_0 + J_0(t - t_0) + \tfrac{1}{2}S_0(t - t_0)^2 \tag{1}$$

$$V = V_0 + \int_0^t A\,dt$$

$$R = R_0 + \int_0^t V\,dt \tag{2}$$

where the subscript i represents the vehicle local x, y, or z directional channel (for this study x is the vehicle downrange direction, y is the vehicle crossrange direction, and z is the vehicle vertical direction). The coefficients of the acceleration polynomial are computed by constraining the trajectory to the initial and final boundary conditions.

One form of the thrust equations derived from the approach above is as follows (the reader is directed to Refs. 9–12 for a detailed derivation and alternate forms): setting $T_{go} = t - t_0$, where t_0 is the current time and t is the time at touchdown, the object is to find the final time t that shapes the descent trajectory using the following relations:

$$F_i = \frac{-6A_{it}}{T_{go}} - \left(\frac{18V_{it}}{T_{go}^2} + \frac{6V_i}{T_{go}^2}\right) + \frac{24(R_i - R_{it})}{T_{go}^3} \tag{3}$$

$$D_i = \frac{6A_{it}}{T_{go}^2} + \left(\frac{36V_{it}}{T_{go}^3} + \frac{12V_i}{T_{go}^3}\right) - \frac{72(R_i - R_{it})}{T_{go}^4} \tag{4}$$

$$T_{go\,new} = T_{go} + \frac{J_{it} - F_i}{D_i} \tag{5}$$

where F_i is the jerk (the time derivative of acceleration) and D_i is the partial derivative of the jerk with respect to T_{go}. The time to go (T_{go}) that satisfies the required final value of F_i is found by iterating on the difference between F_i and D_i as a function of T_{go}, until a zero difference between $T_{go\,new}$ and T_{go} is achieved. Once this zero difference is found, T_{go} becomes the new elapsed time required to reach the terminal target based on the current-state and the terminal-state conditions at each point in the trajectory. The desired final time t is found using $t = t_0 + T_{go}$. Once T_{go} is found, the thrust commands are computed using the following expressions:

$$\begin{bmatrix} T_x \\ T_y \\ T_z \end{bmatrix} = \begin{bmatrix} 0 & \frac{24}{T_{go}^3} & \frac{-72}{T_{go}^4} \\ 0 & \frac{-6}{T_{go}^2} & \frac{24}{T_{go}^3} \\ 1 & \frac{6}{T_{go}} & \frac{-12}{T_{go}^2} \end{bmatrix} \begin{bmatrix} A_{it} \\ V_{it} - V_i \\ R_{it} - R_i - V_i T_{go} \end{bmatrix} \tag{6}$$

A simplified form can be found using the following approach. The terminal boundary conditions are the desired terminal conditions with respect to the landing target and are set equal to zero. Assuming that the terminal jerk condition is zero and the only terminal acceleration condition is the gravitational acceleration (acceleration constraint in the vehicle vertical direction), the problem simplifies to

$$T_{go} = -\frac{1}{2}\frac{V_i + \sqrt{V_i^2 + 16R_i g}}{g}, \qquad i = x, y, \text{ or } z \tag{7}$$

$$T_x = \frac{6V_x}{T_{go}} - \frac{12R_x}{T_{go}^2} \tag{8}$$

$$T_y = \frac{6V_y}{T_{go}} - \frac{12R_y}{T_{go}^2} \tag{9}$$

$$T_z = \frac{6V_z}{T_{go}} - \frac{12R_z}{T_{go}^2} + g \tag{10}$$

Investigating the equations above, one can see that T_{go}, T_x, T_y, T_z are functions of the relative velocity components (V_x, V_y, and V_z), which change with the changing winds. Therefore, wind gusts will alter the T_{go} values and the thrust commands. Also notice that the T_{go} equation is a function of only one channel x, y, or z. The z channel was selected because of its smaller wind deviations (to be addressed later in this paper).

For comparison, the primary objective of the terminal descent navigator on the Viking lander was to converge on an accurate estimate of the altitude relative to the local Mars surface prior to the parachute deployment.[11,12] During terminal descent the attitude control laws drove the lateral body velocities to zero. Thus, the velocity vector was aligned with the lander longitudinal axis. The

longitudinal axis thrust was adjusted to track a prestored velocity-altitude contour with no specific requirement on the crossrange (or lateral) directions. This resulted in a gravity turn guidance that was fuel-optimal and converged to a vertical descent as the lander approached touchdown. However, it offered no obstacle maneuvering in the crossrange channel such as the E guidance shown above. The Viking missions had a landing accuracy requirement of approximately 300 km downrange and 180 km crossrange.

Propulsion Performance

The MRSR lander's propellant tanks were baselined to be sized for 350 m/s of ΔV. This should provide a crossrange capability of 1–2.5 km with the power descent beginning at 1.5-km altitude. The maximum T/W baselined in Ref. 5 is 3.00 using Mars gravity (approximately 1.14 for Earth). However, as will be shown, a maximum T/W of 4.00 appears to offer a more robust lander, especially for density dispersions.

Landing Profile

The landing sequence is defined in this paper as beginning at the end of the entry phase and starting with parachute deployment. A parachute is deployed at an altitude of 3 to 5 km above the terrain. The parachute phase is a ballistic trajectory where the only control available is the timing of the parachute deployment and jettison. At deployment, the lander will have a Mach number of approximately 1.5, depending on the entry-vehicle trajectory design, and a dynamic pressure of 1500 N/m^2. After the lander descends on the parachute to an altitude of 1.5 to 2.0 km and a velocity of about 120 m/s, the parachute is jettisoned and the powered descent phase of the landing begins. Since the lander was ballistic during the parachute phase, its trajectory will be perturbed away from the nominal preplanned trajectory, primarily by surface winds/gusts, density dispersions, and timing errors at deployment and jettison. Once the lander is off the parachute and able to maneuver with power, it will remove the trajectory deviations accumulated while on the parachute. An in-depth discussion of the total landing scenario from the deorbit burn to touchdown can be found in Ref. 5.

Trajectory Dispersion Analysis During Terminal Landing

This investigation covered four different perturbations, all compared with respect to the total ΔV and maximum T/W required during the powered descent phase for a "soft" or a "pinpoint" landing. A soft landing is defined as one where the touchdown velocity is less than 1 m/s, and a pinpoint landing is defined as one where the vehicle lands within 10 m of the terminal target. The four different perturbation areas covered are:

1) Constant headwind/tailwind and crosswind in the terminal landing area. Their speeds are varied from 0 to 60 m/s.

2) Randomly varying headwinds/tailwinds. Headwinds, tailwinds, crosswinds, and updrafts are represented by stochastic models similar to the Dryden wind-gust model.

3) Random density variations off a nominal density profile—a first-order Gauss-Markov model is used to vary the density randomly by ±30% to or ±60% off nominal. The nominal selected model is the mean northern summer COSPAR model.

4) Time on the parachute (varying parachute jettison altitudes). The amount of time the vehicle is allowed to remain on the parachute is varied from 0 (pure power descent) to the nominal 30 s.

For all of the investigations below, it is assumed that the landing vehicle knows the position of the target area (no navigation error). The landing vehicle is required to execute a soft pinpoint landing. For comparison, the Viking missions had a landing accuracy requirement of approximately 300 km downrange and 180 km crossrange and were concerned only with achieving a soft touchdown. A fully integrated guidance, navigation, and control (GN&C) three-degree-of-freedom simulation is utilized. No flight controller error is assumed for this study. Since the primary purpose of this investigation is to study the density and wind effects during the final phases (parachute and powered descent phases) of the landing, the simulation starts at parachute deployment and terminates upon surface touchdown. State conditions at the start of each phase are given in Table 1.

Wind Dispersions During Terminal Landing

One of the most comprehensive models of the winds of Mars is the Mars GRAM model.[13] According to Ref. 13, there is no actual profile of wind velocity versus altitude available for the Mars atmosphere. Therefore, the author of Ref. 13 constructed such profiles using thermal wind relations based on actual temperature profiles of the Martian atmosphere. The temperature profiles were derived from the Viking and Mariner spacecraft radio occultation observations. The full explanation of this relationship between the wind velocities and temperature is beyond the scope of this study; however, a brief discussion follows. Basically, the thermal wind relations imply that the vertical gradient in the zonal winds, across a given altitude layer, is proportional to the meridional gradient in the layer-average temperature.

In Ref. 13, the author constructs a wind profile for the mid-spring season using the Mars GRAM and compares it with Mariner 9 data.[14] The GRAM model shows a strong jet near 5-km altitude and 70°N latitude with winds from the west reaching velocities up to 100 m/s. The Mariner data do not indicate a wind velocity this large; they depict zonal winds up to approximately 20 m/s. It is pointed out by the author of Ref. 13 that both the Mariner 9 and the GRAM wind profiles are derived using available data and thermal wind relations. It is further pointed out that the disagreement in the strong jet near 70°N latitude may indicate a problem with the GRAM temperature parametrizations near this latitude. However, since there are no actual data to compare from either analysis, the high winds of the GRAM model must be considered. The Mariner 9 data and the GRAM model agree on winds with velocities reaching up to 50–60 m/s at 5-km altitude and 50°S latitude. Actual surface wind data for the Viking lander data sites can be found Ref. 15. According to Ref. 15, surface winds at the landing sites reached speeds up to approximately ±20 m/s for both zonal and meridional wind directions. For comparison, the GRAM model calculates surface zonal winds up to ±50 m/s, and the Mariner 9 analysis calculates winds up to ±15 m/s.

Since actual wind data are not available for the entire surface of Mars (being available only at the Viking and Mariner landing sites), and since the lander investigated in this report may be required to land at any point on the surface, it was concluded that the ±60 m/s wind velocities that encompass both the GRAM and Mariner 9 models will be treated as the 3σ zonal wind boundaries for this investigation. Based upon the GRAM model and Viking data, the 3σ meridional and vertical wind gusts were selected to be ±40 m/s and ±20 m/s, respectively.

Constant Headwind/Tailwind and Crosswind

Constant headwinds and tailwinds were investigated because the lander may penetrate a weather front that includes a strong wind

Table 1 State conditions at the start of each phase

	Parachute phase	Powered descent phase
Initial altitude, km	5 (chute deployment)	1.5 (chute jettison)
Initial downrange to target, km	10	1.5
Initial relative velocity, m/s	500	120
Initial flight path angle, deg	−10	−45
Mass, kg	4082	3600
Ballistic coeff., kg/m^2	28 (aeroshell vehicle + chute)	2600 (lander vehicle)
Approximate time in phase, s	40 (on chute)	30 (powered descent)

Table 2 Results of Monte Carlo analysis of wind-gust ΔV and maximum T/W

Wavelength of gust, m	Mean ΔV required, m/s	3σ deviation of ΔV required, m/s	Mean maximum T/W required, m/s	3σ deviation of maximum T/W, m/s
500	212.154	4.257	2.253	0.219
5,000	217.879	10.939	2.453	0.349
50,000	215.394	7.668	2.368	0.308

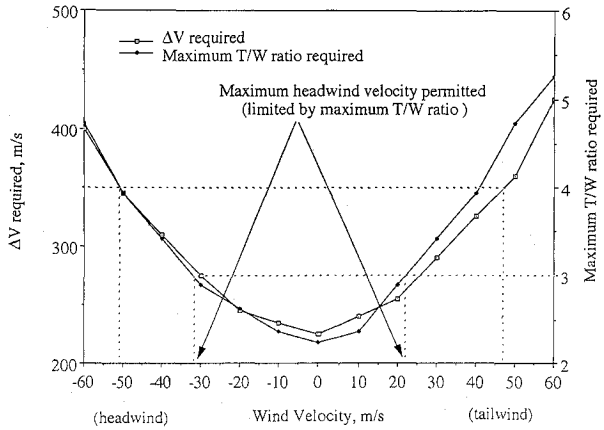

Fig. 1 ΔV and maximum T/W vs headwind and tailwind velocities.

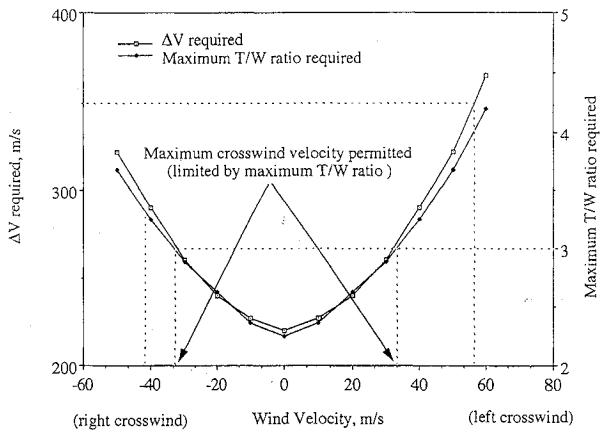

Fig. 2 ΔV and maximum T/W vs crosswind velocities.

shift just prior to parachute deployment. This would be a worst-case scenario in that, prior to parachute deployment during the aeroshell entry phase, the lander has the possibility of maneuvering to remove wind dispersions, whereas during the parachute phase the lander is at the mercy of the winds, with only the terminal descent engines to remove the dispersions after parachute jettison. The influences of headwinds/tailwinds on the lander are shown in Fig. 1, and the influences of crosswinds are shown in Fig. 2.

As seen in Fig. 1, the stronger headwinds require larger ΔV and T/W. Greater values of ΔV are required because of the decrease in forward relative velocity as the headwind velocity increases. The vehicle is traveling due east. Therefore, a headwind is an easterly wind and has a negative value (east is the direction from which the wind is coming). According to baseline designs, headwinds up to 32 m/s are allowed and are limited by the maximum T/W allowed. Tailwinds greater than 22 m/s attempt to carry the vehicle beyond the landing target, causing it to reverse its direction of travel. This results in large changes in forward momentum that require large amounts of thrust. It can be seen that if the maximum T/W were increased to 4.00, headwinds up to 52 m/s and tailwinds up to 46 m/s would be allowed.

As seen in Fig. 2, the stronger crosswinds require larger than nominal ΔV with a matching trend increase in the maximum required T/W. Greater values of ΔV are required because of the increasing drag as the crosswind velocity increases. The vehicle is traveling due east. Therefore, a north crosswind has a positive value (north is the direction from which the wind is coming and is to the left of the vehicle's direction of travel). Again, if the maximum T/W were increased to 4.00, crosswinds up to 55 m/s would be allowed. See Fig. 2.

Randomly Varying Headwinds/Tailwinds

A Gauss-Markov stochastic wind model is derived using a form analogous to the Dryden wind-gust model. A wideband white-noise source with a specified power spectral density function (PSD) $\Phi_n(\omega)$ is passed through linear filters to achieve the appropriate wind-gust model. A PSD model for each of the downrange, crossrange, and vertical channels is constructed in the following form:

$$\Phi_u(\omega) = 2\sigma_u^2 \frac{L_u}{\pi U_0} \frac{1}{1 + (L_u^2/U_0)\omega^2} \tag{11}$$

$$\Phi_v(\omega) = \sigma_v^2 \frac{L_v}{\pi U_0} \frac{1 + 3(L_v^2/U_0)\omega^2}{1 + (L_v^2/U_0)\omega^2} \tag{12}$$

$$\Phi_w(\omega) = \sigma_w^2 \frac{L_w}{\pi U_0} \frac{1 + 3(L_w^2/U_0)\omega^2}{1 + (L_w^2/U_0)\omega^2} \tag{13}$$

Three sets of 1000-run Monte Carlo investigations are performed using the wind-gust model above. The difference in the three sets is in the wavelength of the wind gust. Gust wavelengths (which select the intensity of the gust) of 500, 5000, and 50,000 m are investigated. Using the following relations, the intensity of the wind gusts can be found for those wavelengths, respectively:

$$\frac{\sigma_u^2}{L_u} = \text{downrange intensity} = 7.200, 0.720, 0.072 \text{ m/s}^2$$

$$\frac{\sigma_v^2}{L_v} = \text{crossrange intensity} = 3.200, 0.320, 0.032 \text{ m/s}^2$$

$$\frac{\sigma_w^2}{L_w} = \text{vertical intensity} = 0.800, 0.080, 0.008 \text{ m/s}^2$$

As explained above, ±60-m/s wind velocities are treated as the 3σ zonal wind boundaries, and the 3σ meridional and vertical wind-gusts are selected to be ±40 and ±20 m/s, respectively.

Table 2 shows that the 3σ wind velocities do not appreciably affect the landing performance for any of the three gust intensities investigated. Gust wavelengths of 5000 m have the largest influence on the required ΔV and maximum T/W. Referring to Table 2, a 3σ ΔV of 228.8 m/s and a 3σ maximum T/W of 2.80 are found to be adequate for all the winds investigated. Any additional maneuvering, such as obstacle avoidance, will require additional ΔV. However, the maximum T/W of 2.8 should be sufficient to null out wind dispersions during the hazard-avoidance maneuvering.

Random Varying Density

A first-order Gauss-Markov stochastic density model is also derived. The following autocorrelation is used to emulate density perturbations:

$$\varphi_{\rho\rho}(\Delta h) = \sigma_\rho^2 \exp(-\beta|\Delta h|) \tag{14}$$

The Viking 1 vehicle found deviations in atmospheric density of −7.5% to 0.0% with respect to the COSPAR northern hemisphere mean model during terminal descent (5 km and below), and the Viking 2 found −4.0% to +3.0% deviations. According to Ref. 15, the Viking lander data are used to construct altitude

Table 3 Results of Monte Carlo analysis of density dispersion ΔV and maximum T/W

Wavelength of deviation, m	Initial 1σ density deviation,%	Mean ΔV required, m/s	3σ deviation of ΔV required, m/s	Mean maximum T/W required, m/s	3σ deviation of maximum T/W, m/s
100	±30	216.060	11.454	2.434	0.358
1000	±30	214.378	9.644	2.374	0.333
100	±60	225.735	22.376	2.857	0.750
1000	±60	219.002	13.287	2.521	0.375

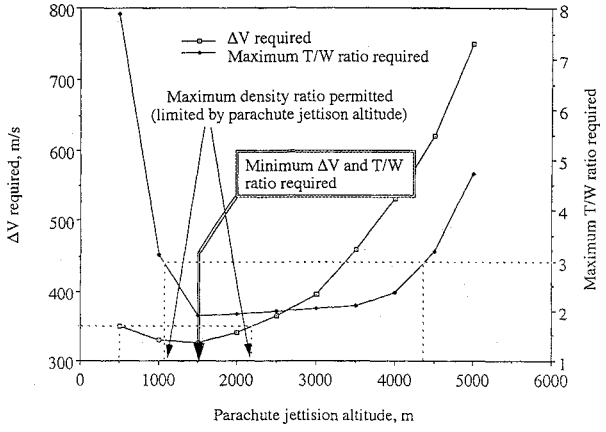

Fig. 3 ΔV and maximum T/W vs parachute jettison altitude.

density-deviation models. The models constructed are the results of one-dimensional circulation computations and are based on the lower boundary conditions at the Viking 1 and 2 lander locations. For altitudes of 5 km and below, the models give maximum density deviations of −15% to +30%. From this derived model and the Viking information above, two density-deviation models are considered for this study: ±30% and ±60% (1σ). Also, two different density dispersion wavelengths were investigated: 100 and 1000 m. Four sets of 1000-run Monte-Carlo investigations were performed using the density deviations and density wavelengths given above. Table 3 shows the effect of the density deviation on the ΔV required and the maximum T/W required.

Table 3 shows that density changes have a very large effect on the maximum T/W required, on account of the small ballistic coefficient (compared to the lander) of the parachute. An increased density profile causes the parachute to be more effective (creates a greater drag force) and thus causes the vehicle to fall short of the nominal-density-profile trajectory. Falling short of the nominal trajectory requires the vehicle to propel itself further in order to achieve touchdown at the landing target. The T/W and ΔV are especially affected by a density profile less than the nominal, because in that case the parachute is not very effective and the vehicle attempts to fly beyond the landing target. This requires the vehicle to change direction (change in forward momentum) for return to the target. Density dispersion wavelengths of 100 m had a greater influence on the required ΔV and maximum T/W than the 1000-m gust wavelengths, because of the larger density-deviation intensity of the 100-m wavelength. Referring to Table 3, a 3σ ΔV of 248.1 m/s and a 3σ maximum T/W of 3.6 should be able to tolerate any of the density dispersions investigated in this study. These requirements are greater than the wind-gust requirements. This stresses the fact that atmospheric density dispersions (which according to Ref. 15 can vary as much as 15% between morning and evening) can have a large effect on lander-vehicle engine sizing and fuel requirements.

Another serious contributor, not considered in this report, is the effect of density shears and buckets on trajectory accuracy.

Parachute Jettison Altitudes

Various parachute jettison altitudes, all using the same 5-km deployment altitude, are investigated. Figure 3 shows that jettisoning the parachute at altitudes greater than, or less than, 1.5 km increases the amount of ΔV and maximum T/W required. This graph gives a measure of how long the vehicle remains on the parachute versus ΔV and maximum T/W. Staying on the parachute for 30 s (parachute deployment at 5 km and jettison at 1.5 km) requires the least ΔV and least maximum T/W.

Landing Capabilities for Navigation Trajectory Maneuvers

An in-depth discussion of the navigation error contributions to the total landing dispersion errors can be found in Ref. 16. In summary, navigation based upon Earth-relative navigation sensors, such as the Deep Space Network (DSN), incorporate inertial-map errors (tying the Earth inertial frame to the planetary-landing-site inertial frame) and cannot be used for real-time navigation for that reason as well as, for most planetary bodies, the lengthy transmission times between the Earth and the planet. The difference between the two inertial coordinate frames (inertial-map error or frame tie error) for the MRSR mission is estimated to be 500–1000 m. Therefore, assuming the lander is using a hypothetically error-free inertial measurement unit (IMU) during descent and landing, the descent and landing trajectory will include the inertial-map error. This results in a terminal landing navigation position error of no less than the inertial-map error. In order to achieve pinpoint landings, a planet-relative (or more specifically, target/surface-relative) navigation method (such as SAR) must be used. Also, it is well known that angle measurements, resulting from surface feature navigation (terrain scene matching), can reduce navigation errors substantially.

Both the hazard-avoidance and the precision-landing navigation methods may require some form of terrain scene matching and/or recognition such as SAR. The accuracy of either method can be seriously degraded if viewing of the surface performed during the descent to the surface is poor. Also, SAR delivers much greater accuracy when not approaching the final landing point straight on. In fact, it must see the target moving out of the altitude-downrange plane in order to function properly.[17] An off-the-flight-path "squint" angle is required so that the SAR imager can see the terrain it is imaging from various perspectives, which are used to construct a 3D image of the area being observed. This out-of-plane navigation results in the SAR instrument observing the surface with an azimuth (or squint) angle. SAR imaging normal operations require a minimum of 10 deg and a maximum of 50 deg; average sensor scenes are routinely imaged at 45 deg off the flight path.

Because SAR is being considered for terminal navigation of the MRSR lander, a study is conducted to investigate the possibility of the lander aeroshell maneuvering slightly away from the landing point in order to establish the squint angle. Once the landing-point navigation fix is properly established, the aeroshell vehicle turns back towards the landing point and deploys the parachute, and the lander completes the landing. A study is conducted to investigate the capabilities of the aeroshell in establishing a proper squint angle. It should be noted that the lander vehicle has very little fuel for maneuvering. Therefore, altering the aeroshell trajectory so that it has more energy (velocity) during the azimuth phase and using it to perform the SAR navigation maneuvers is considered the optimal fuel-conserving method. Performing navigation before the parachute phase allows navigation error to build up while the vehicle is on the parachute. However, the primary purpose of the landmark navigation is to remove the inertial-map error, and this can be accomplished during the azimuth phase. The navigation errors acquired during the parachute phase should be minimal compared to the inertial-map error and can be removed by having the lander vehicle perform navigation updates during powered descent.

The study investigates a target that is located at some lateral distance away from the deadband direction (straight-line direction from the vehicle to the target established in the altitude/downrange plane).

Table 4 Approximate initial conditions at each phase of descent and landing

Phase	Time, s	Initial alt., m	Initial vel.,[a] m/s	Initial FPA,[a] deg	Guidance used	Other
Deorbit	−2280.0	500,000.0	3115.0 (I)	0.0 (I)	None	ΔV burn 200m/s
Entry	0.0	125,000.0	3350.0 (I)	−3.3 (I)	MPEG[5]	Entry interface (EI)
Azimuth	1261.0	25,000.0	1145.0 (R)	−2.4 (R)	AZ	Mass 4082 kg
Parachute	1521.0	3,000.0	350.0 (R)	−8.2 (R)	None	Mach 1.5 at deploy
Power	1561.0	1,500.0	120.0 (R)	−15.0 (R)	LEM	Mass 3600 kg
Touchdown	1583.0	0.0	1.0	−90.0 (R)	LEM	ΔV limit 350 m/s

[a]R: relative to planet surface; I: inertial; FPA: denotes flight-path angle.

Table 5 Results of turn-to-target investigations

Slantrange from target, m	Downrange to chute deploy, m	Altitude, m	Velocity, m/s	Complete turn to target, s
10,000	3,200	3,500	482	4–5
20,000	13,200	5,300	537	21–23
30,000	23,200	7,200	585	32–33
40,000	33,200	9,100	635	40–42
50,000	43,200	11,000	677	46–48
60,000	53,200	13,000	717	51–54

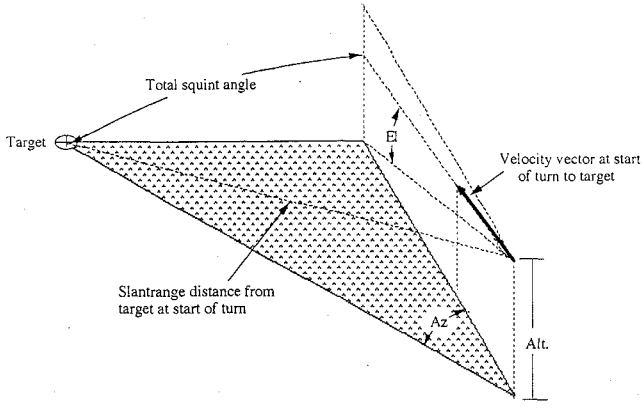

Fig. 4 Geometry of azimuth and elevation measurements.

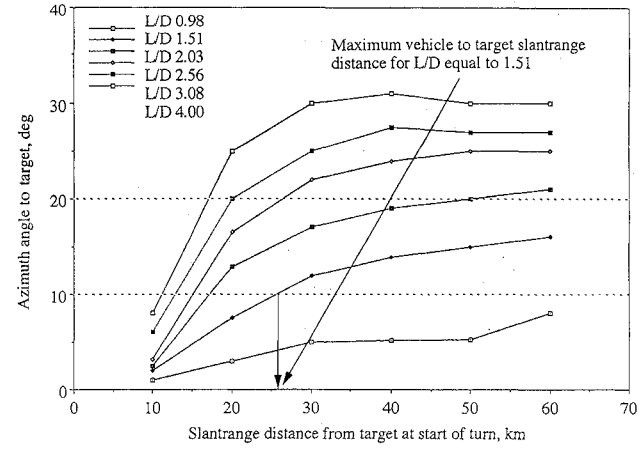

Fig. 5 Azimuth angle to target vs distance from target at start of turn.

This crossrange differential is removed during the approach phase before parachute deployment. Parachute deployment occurs at an altitude of 3000 m, and powered descent is initiated at 1500 m. The rationale of lowering the parachute deployment altitude 2000 m from the nominal deployment altitude of 5000 m is to allow more maneuvering room for the aeroshell vehicle.

In order to assess the feasibility of using line-of-sight navigation from the vehicle to the target, investigations into acquisition of line-of-sight capabilities are investigated. For a typical entry trajectory, line-of-sight contact first occurs at approximately 450 km downrange and 31 km in altitude. (Note: a perfectly smooth and spherical planet is used for the line-of-sight calculations.) Therefore, the target (landing point) is in view during the azimuth phase. For this azimuth navigation study the entry/landing trajectory is divided into six phases. The initial conditions for each of these phases are given in Table 4.

The final approach turn to target occurs towards the end of the azimuth control phase after the SAR navigation updates occur. During that time, an azimuth controller is used to direct the velocity vector towards the direction of the target starting at a selected slant range from the target. At this slant-range distance, the L/D of the vehicle is kept constant or altered from the original 0.98 up to 4.00, and the turn is initiated. The increase in the L/D is used to study the turning capabilities of the vehicle as a function of its lifting capability. It is found early in the study that an L/D of 0.98 allows only a small amount of maneuvering—so small that SAR may not be possible. Therefore, it is decided that the L/D (more specifically, the coefficient of lift C_L) may need to be altered in order to obtain proper maneuvering performance.

The turn is continued until the 3000-m parachute deployment altitude is achieved. At this point, the vehicle is headed straight toward the target and the parachute is deployed. The turning capability of the aeroshell vehicle is measured by finding the maximum azimuth and elevation angle that allow the vehicle to successfully arrive at the target once the turn to the target is initiated. Figure 4 shows the angles of interest with respect to the vehicle and landing-site target. Results of the analysis can be found in Fig. 5. From Fig. 5 one can see that a vehicle with a minimum L/D of 1.51 and starting the turn to the target at 26 km away has gives an instantaneous azimuth angle of 10 deg before the vehicle must turn towards the target. Therefore, an L/D of 1.51 (50% greater than baseline) is the minimum that the aeroshell vehicle can have when using azimuth measurements for SAR navigation. The change-in-elevation capability depends negligibly on L/D.

Starting the final turn toward the target at distances from the target of 20 km or less greatly reduced the turning capability of the vehicle, to the point that it could not make it to the target. This was because the vehicle did not have enough time (or downrange distance to the target) to establish a reasonable turn rate (see Table 5).

It can be seen that changes in the L/D of the aeroshell vehicle have very little influence on the amount of elevation angle achieved. This is because the additional lift from the increased L/D is used for side forces to increase the amount of azimuth change achievable. The amount of vehicle crossrange maneuvering is given in Table 6 for a variety of L/D values and different slant-range distances from the target where the turn is initiated.

It should be noted that the results obtained in this investigation are found using a three-degree-of-freedom simulation where all turning rates were assumed to be instantaneous. In actual flight, the turning rates would not be instantaneous but would ramp up. However, the results of this investigation (although optimistic) allow a comparison

Table 6 Aeroshell-vehicle crossrange capabilities

Slantrange from target, m	L/D of vehicle	Crossrange distance achieved in turn, m
10,000	0.98	114
30,000	0.98	2,100
50,000	0.98	4,800
10,000	2.03	330
30,000	2.03	6,500
50,000	2.03	14,000
10,000	3.08	500
30,000	3.08	10,000
50,000	3.08	23,000

of the vehicle configuration and trajectory on the landing accuracy, fuel requirements, etc., of the landing scenario.

Conclusions

This study concludes that current Mars mission designs, such as MRSR-type designs (limiting the total ΔV used to 350 m/s and the maximum Mars T/W to 3.00), allow frontal wind shifts consisting of headwinds up to 32 m/s, tailwinds up to 22 m/s, and crosswinds up to 33 m/s. Actual measurements from the Viking 2 spacecraft found headwinds up to 17.4 m/s, tailwinds up to 20 m/s, and crosswinds up to 17.6 m/s. It was found that tailwinds of 22 m/s and greater, or densities less than a nominal density profile, cause the vehicle to fly beyond the target landing area. This fly-by required the landing vehicle to expend large amounts of fuel to return to the landing target.

A ΔV of 248.1 m/s and a maximum T/W of 3.6 are required for random wind and density deviations, mainly on account of the density dispersions. It was found that the lander T/W is more sensitive to density dispersions than to wind deviations. Most of the dispersions take place during the parachute phase, because of its small ballistic coefficient compared to that of the landing vehicle during the terminal landing phase. A parachute jettison altitude range of 1050 to 2250 m (with deployment at 5 km) allows the lander to stay within the baseline T/W and ΔV requirements. A parachute jettison altitude of 1500 m requires the least ΔV and T/W.

For terminal navigation maneuvers during the azimuth phase, starting the final turn toward the target, at target distances of 20 km or less, greatly reduces the turning capabilities of the vehicle. This is because of the vehicle not having enough time to turn. A vehicle L/D of 0.98 results in a low lift force component for use in turning the vehicle. This is because most of the lift force is required to counteract the gravitational pull of Mars, leaving very little for the side (turning) component. An L/D of 1.51 (50% greater than baseline) is the minimum that aeroshell vehicle can have when using azimuth measurements for SAR navigation, assuming a nearly instantaneous SAR navigation update. Therefore, unless alteration of the aeroshell can be used to increase the L/D without substantially changing the overall design, using the aeroshell to perform maneuvers for navigation purposes during the final phases of the flight is not recommended.

Acknowledgment

The author gratefully acknowledges the support of the state of Texas for this research under the Advanced Technology Program, Grant 003656089.

References

[1]Draper, R. F., "The Mariner Mars 11 Program, " AIAA Paper 88-0067, Jan. 1988.

[2]Bourke, R. D., Kwok, J. H., and Friedlander, A., "Mars Rover Sample Return Mission," AIAA Paper 89-0417, Jan. 1989.

[3]Carter, P. H., and Smith, R. S., "Mars Rover Sample Return Lander Performance," AIAA Paper 89-0633, Jan. 1989.

[4]Pivirotto, D. S., Penn, T. J., and Dias, W. C., "Mars Rover 1988 Concepts," AIAA Paper 89-0419, Jan. 1989.

[5]Gamble, J., "JSC Pre-Phase A Study Mars Rover Sample Return Mission, Aerocapture, Entry and Landing," NASA CR-23230, May 1989.

[6]Whitlock, C. H., and Bendura, R. J., "Inflation and Performance of Three Parachute Configurations from Supersonic Flight Test in a Low Density Environment," NASA-TN-D-5296, July 1969.

[7]Cherry, G. W., "*E* Guidance—A General Explicit Optimizing Guidance Law for Rocket-Propelled Spacecraft," MIT Instrumentation Lab., Report R-456, Boston, MA, Aug. 1964.

[8]Klumpp, A. R., "A Manually Retargeted Automatic Descent and Landing System for LEM," MIT Instrumentation Lab., Report R-539, Boston, MA, Mar. 1966.

[9]Klumpp, A. R., "A Manually Retargeted Automatic Landing System for the Lunar Module (LM)," *Journal of Spacecraft and Rockets*, Vol. 5, No. 2, Feb. 1968, pp. 129–138.

[10]Klumpp, A. R., "Apollo Lunar Descent Guidance," Charles Stark Draper Labs., R-695, Cambridge, MA, June 1980.

[11]Ingoldby, R. N., "Guidance and Control Design of the Viking Planetary Lander," *Journal of Spacecraft and Rockets*, Vol. 1, No. 3, 1978, pp. 189–196.

[12]Holmberg, N. A., Faust, R. P., and Holt, H. M., "Viking '75 Spacecraft Design and Test Summary: Vol. I—Lander Design," NASA-RP-1027, Nov. 1980.

[13]Justus, C. G., "Mars Global Reference Atmosphere Model for Mission Planning and Analysis," *Journal of Spacecraft and Rockets*, Vol. 28, No. 2, 1991, pp. 216–221.

[14]Leovy, C., "Martian Meteorological Variability," *Advances in Space Research*, Vol. 2, Nov. 1982, pp. 19–44.

[15]Kaplan, D., "Environment of Mars, 1988," NASA-TM-D-100470, Oct. 1988.

[16]Tuckness, D. G., "Imaging Penetrator Beacon Design for Mars," *Journal of Spacecraft and Rockets*, Vol. 31, No. 6, 1994, pp. 1123–1129.

[17]Henry, J. C., "35 GHz SAR Images Created by the Advanced Detection Technology Sensor(s)," Record of the 34th Annual Tri-Service Radar Symposium(s), Air Force Wright Aeronautical Labs., TR-88-1112, June 1988.